materials

MDPI

Article

Influence of Pd Doping on Electrical and Thermal Properties of *n*-Type $Cu_{0.008}Bi_2Te_{2.7}Se_{0.3}$ Alloys

Se Yun Kim [1,†], Hyun-Sik Kim [2,†], Kyu Hyoung Lee [3], Hyun-jun Cho [4], Sung-sil Choo [4], Seok-won Hong [4], Yeseong Oh [4], Yerim Yang [4], Kimoon Lee [5], Jae-Hong Lim [6], Soon-Mok Choi [7], Hee Jung Park [8], Weon Ho Shin [9,*] and Sang-il Kim [4,*]

1 Samsung Electronics, Suwon 16678, Korea; ksyvip@gmail.com
2 Department of Materials Science and Engineering, Hongik University, Seoul 04066, Korea; hyunsik.kim@hongik.ac.kr
3 Department of Materials Science and Engineering, Yonsei University, Seoul 03722, Korea; khlee2018@yonsei.ac.kr
4 Department of Materials Science and Engineering, University of Seoul, Seoul 02504, Korea; joshua4150@uos.ac.kr (H.-j.C.); cntjdtlf111@uos.ac.kr (S.-s.C.); seokown4926@uos.ac.kr (S.-w.H.); asdf85205@uos.ac.kr (Y.O.); yyl0201@uos.ac.kr (Y.Y.)
5 Department of Physics, Kunsan National University, Gunsan 54150, Korea; kimoon.lee@kunsan.ac.kr
6 Department of Materials Science and Engineering, Gachon University, Seongnam 13120, Korea; limjh@gachon.ac.kr
7 School of Energy, Materials and Chemical Engineering, Korea University of Technology and Education, Cheonan 31253, Korea; smchoi@koreatech.ac.kr
8 Department of Materials Science and Engineering, Dankook University, Cheonan 31116, Korea; parkjang@dankook.ac.kr
9 Department of Electronic Materials Engineering, Kwangwoon University, Seoul 01897, Korea
* Correspondence: weonho@kw.ac.kr (W.H.S.); sang1.kim@uos.ac.kr (S.-i.K.)
† These authors contributed to this work equally.

Received: 18 November 2019; Accepted: 4 December 2019; Published: 6 December 2019

Abstract: Doping is known as an effective way to modify both electrical and thermal transport properties of thermoelectric alloys to enhance their energy conversion efficiency. In this project, we report the effect of Pd doping on the electrical and thermal properties of *n*-type $Cu_{0.008}Bi_2Te_{2.7}Se_{0.3}$ alloys. Pd doping was found to increase the electrical conductivity along with the electron carrier concentration. As a result, the effective mass and power factors also increased upon the Pd doping. While the bipolar thermal conductivity was reduced with the Pd doping due to the increased carrier concentration, the contribution of Pd to point defect phonon scattering on the lattice thermal conductivity was found to be very small. Consequently, Pd doping resulted in an enhanced thermoelectric figure of merit, zT, at a high temperature, due to the enhanced power factor and the reduced bipolar thermal conductivity.

Keywords: thermoelectric; Pd doping; effective mass; bipolar thermal conductivity; phonon scattering

1. Introduction

Thermoelectric alloys have attracted attention in recent decades because these materials can convert a temperature gradient directly into electrical energy. Bismuth telluride (Bi_2Te_3)-based alloys are currently the most used bulk thermoelectric alloys near room temperature [1,2]. However, the broader use of Bi_2Te_3-based alloys is still limited by the rather low thermoelectric conversion performance, evaluated as the thermoelectric figure of merit $zT = \sigma \cdot S^2 \cdot T/\kappa_{tot}$, where σ, S, T, and κ_{tot} are the electrical conductivity, Seebeck coefficient, temperature, and total thermal conductivity, respectively. In fact,

the zT of n-type $Bi_2(Te,Se)_3$ alloys remains below 1, while values significantly higher than 1 have often been reported for p-type $(Bi,Sb)_2Te_3$ alloys.

Doping is an effective approach to improving the zT of Bi_2Te_3 alloys by adjusting the electrical transport properties or reducing the κ through the introduction of additional point defects [3–11]. The zT of p-type $(Bi,Sb)_2Te_3$ alloys can easily be enhanced using substitutional dopants [3–5]. Meanwhile, the influence of doping on n-type $Bi_2(Te,Se)_3$ alloys has not been investigated as much as that of doping on p-type $(Bi,Sb)_2Te_3$ alloys. It has been found that Cu intercalation in n-type $Bi_2(Te,Se)_3$ alloys is a very effective approach to reducing the lattice thermal conductivity (κ_{latt}) by introducing additional point defect scattering centers [12]. However, the accompanying modification of carrier transport properties with the κ_{latt} reduction may reduce the power factor, resulting in zT reduction.

Co-doping of two different substituents was also suggested to further decrease the κ_{latt} while enhancing the power factors in some other thermoelectric materials, such as SnTe and PbTe [13–16]. In p-type $(Bi,Sb)_2Te_3$ alloys, it was found that the co-doping of Ag and Ga reduced the κ_{latt} further compared to that of single doped materials [17], while the power factor can be maintained.

Herein, we investigated the effect of additional Pd substitutional doping on the electrical transport properties and thermal conductivities of Cu-doped n-type $Bi_2(Te,Se)_3$, $Cu_{0.008}Bi_2Te_{2.7}Se_{0.3}$. The Pd was anticipated to scatter phonons effectively due to the large mass and ionic radius differences between Pd and Bi (M_{Pd} = 106.42 u, M_{Bi} = 208.98 u, r_{Pd} = 90 pm, r_{Bi} = 117 pm). Pd doping increased the electron concentration, electrical conductivity, and power factors. However, the contribution of Pd to additional point defect scattering centers on the lattice thermal conductivity was found to be rather small. As a result, zT enhancement due to Pd doping was observed at high temperatures. To investigate the reason for the limited effectiveness of substitutional Pd doping in reducing the κ_{latt} value in n-type $Bi_2(Te,Se)_3$ alloys, the electronic transport properties were analyzed using a single parabolic band model [18], and the reduction in κ_{latt} was quantitatively predicted using the Debye–Callaway model [19].

2. Materials and Methods

The $Cu_{0.008}Bi_2Te_{2.7}Se_{0.3}$ reference sample and a series of Pd-doped $Cu_{0.008}Pd_xBi_{2-x}Te_{2.7}Se_{0.3}$ (x = 0.002, 0.004, 0.01, and 0.02) samples were synthesized by a conventional solid state reaction for 10 h at 1423 K, using high-purity (99.999%) raw materials. The synthesized ingots were ball-milled using a 8000M Mixer/Mill high-energy ball mill (SPEX SamplePrep, Metuchen, NJ, USA) for 10 min, and sieved powders under 45 μm were consolidated by spark plasma sintering at 723 K and 50 MPa for 2 min. Then, the temperature-dependent S and σ parameters were measured over the temperature range between room temperature and 480 K in a direction perpendicular to the pressing direction (ZEM-3, Advanced-RIKO, Yokohama, Japan). The carrier concentrations were determined by Hall measurements in van der Pauw configuration, in a magnetic field of 0.5 T (AHT-55T5, Ecopia, Anyang, South Korea) in the same direction. The κ values of the samples were calculated from their theoretical density (ρ_s), heat capacity (C_p), and thermal diffusivity (λ) values ($\kappa = \rho_s \cdot C_p \cdot \lambda$), measured along the same direction.

3. Results and Discussion

Figure 1a shows the X-ray Diffraction (XRD) patterns of the investigated series of $Cu_{0.008}Pd_xBi_{2-x}Te_{2.7}Se_{0.3}$. All samples showed single phases without impurities. The lattice parameters a and c are shown in Figure 1b, which reveals that the c parameter generally increased with the Pd doping, while a remained largely unchanged upon doping. The systematic change in the c parameter implies that substitutional doping was successfully achieved.

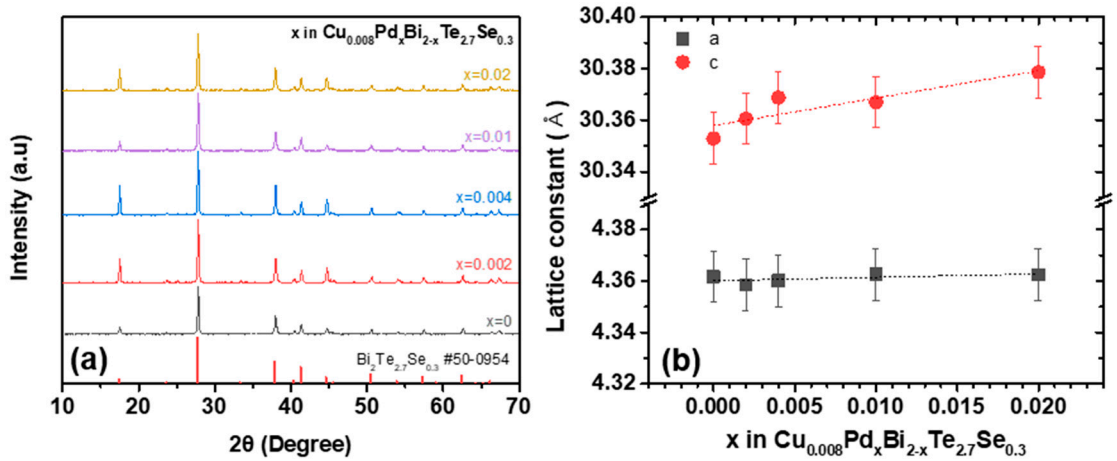

Figure 1. (**a**) X-ray diffraction patterns and (**b**) calculated lattice parameters *a* and *c* of $Cu_{0.008}Pd_xBi_{2-x}Te_{2.7}Se_{0.3}$ (x = 0, 0.002, 0.004, 0.01, and 0.02).

The measured σ and S values of the Pd-doped $Cu_{0.008}Pd_xBi_{2-x}Te_{2.7}Se_{0.3}$ (x = 0, 0.002, 0.004, 0.01, and 0.02) are shown in Figure 2a,b. The σ value of the undoped sample was about 740 S/cm at 300 K, and substantially increased to 1320 S/cm for x = 0.02. On the other hand, the magnitude of the S values at 300 K decreased from −192 to −144 μV/K. As a result, the power factor ($S^2 \cdot \sigma$) at 300 K remained unchanged (around 2.73 mW/m·K^2) regardless of the Pd doping level (Figure 2c). However, an enhancement in the power factor was observed at high temperatures upon Pd doping. For example, at 480 K the power factor was enhanced by 19%, from 1.68 to 2.00 mW/m·K^2.

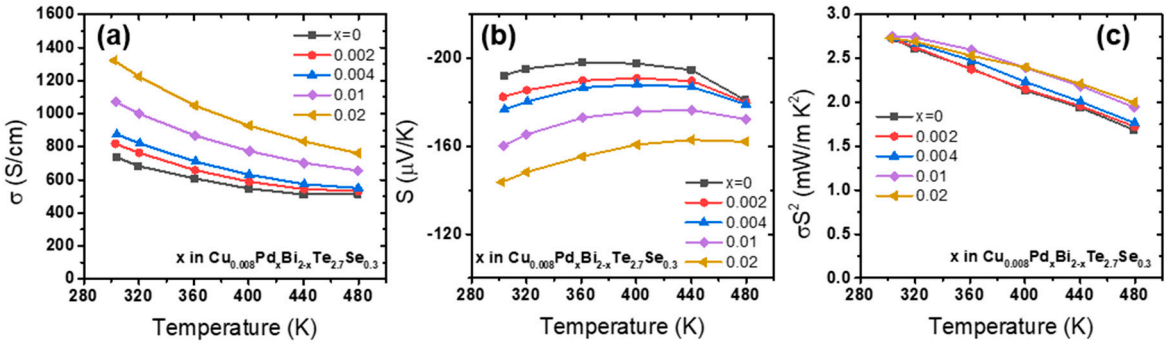

Figure 2. (**a**) σ, (**b**) S, and (**c**) power factor of $Cu_{0.008}Pd_xBi_{2-x}Te_{2.7}Se_{0.3}$ (x = 0, 0.002, 0.004, 0.01, and 0.02).

Figure 3a shows the electron carrier concentration (n_H) and mobility (μ_H) measured for the $Cu_{0.008}Pd_xBi_{2-x}Te_{2.7}Se_{0.3}$ samples at 300 K. The n_H gradually increased with the Pd doping, with n_H values of 2.4, 2.8, 3.2, 3.4, and 4.2 × 10^{19} cm^{-3} for x = 0, 0.002, 0.004, 0.01, and 0.02, respectively. On the other hand, the μ_H values did not change significantly. Therefore, the increase in σ upon Pd doping is mainly due to the increased n_H values. Figure 3b shows the Pisarenko plot of the samples, displaying the S of samples as a function of n_H at 300 K. The solid lines were obtained for different effective masses (m^* = 0.8, 0.9, and 1.0 m_0, where m_0 is the electron mass) using Equation (1):

$$S = \frac{8\pi^2 k_B{}^2}{3eh^2}\left(\frac{\pi}{3n}\right)^{2/3} m^* T \quad (1)$$

where e, h, and k_B are the elementary charge, Planck's constant, and Boltzmann constant, respectively. The m^* values of all samples, deduced using Equation (1), are plotted in Figure 3b. As shown in the figure, Pd doping resulted in slightly increased m^* values, indicating that the electronic structure of the conduction band of $Cu_{0.008}Bi_2Te_{2.7}Se_{0.3}$ was slightly modified favorably for S.

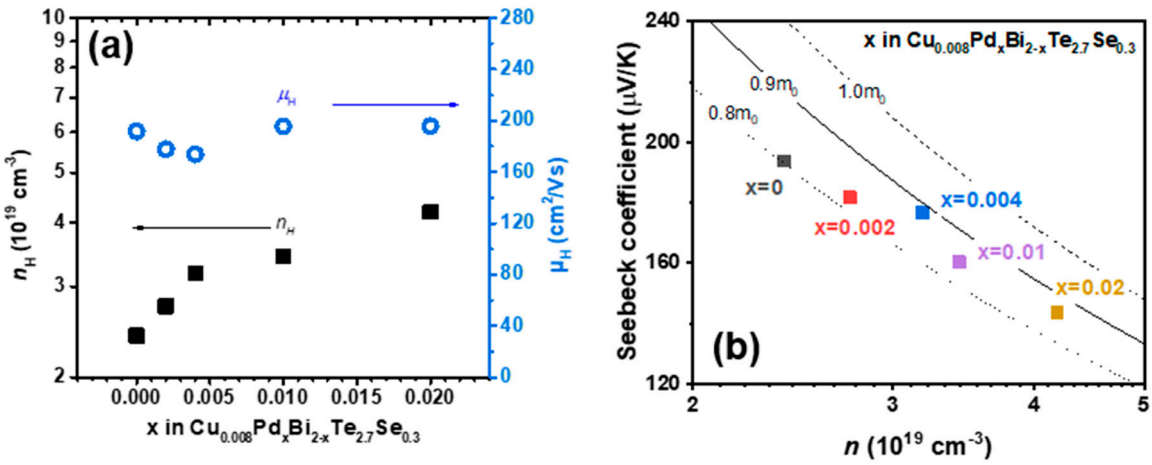

Figure 3. (**a**) Measured carrier concentrations and mobilities and (**b**) Pisarenko plot.

Figure 4a shows the measured κ_{tot} of the Pd-doped $Cu_{0.008}Bi_2Te_{2.7}Se_{0.3}$ samples, revealing that the κ_{tot} values gradually increased with the doping level. In order to understand these changes, we analyzed the contributions to κ_{tot}, given by the following equation:

$$\kappa_{tot} = \kappa_{elec} + \kappa_{bp} + \kappa_{latt} \tag{2}$$

where κ_{elec} and κ_{bp} are the electronic and bipolar thermal conductivities, respectively. First, κ_{elec} was calculated using the equation for the Lorenz number (L, expressed as a simple function with S in Equation (3)) [20], and the results are shown in Figure 4b.

$$L = 1.5 + \exp\left(-\frac{|S|}{116}\right) \tag{3}$$

Equation (3) describes the relationship between the L and S in a simple function, based on a single parabolic band model [20]. The κ_{elec} values increased as the electrical conductivity increased with Pd doping, straightforwardly with the increased carrier concentration (Figure 3a). At 300 K, κ_{elec} showed a significant increase from 0.4 to 0.7 W/m·K.

The κ_{bp} parameter, related to the bipolar electronic transport properties, can be estimated based on a single parabolic band model and the Boltzmann transport equation (Equation (4)):

$$\kappa_{bp} = \left({S_p}^2\sigma_p + {S_n}^2\sigma_n - S^2\sigma\right)T \tag{4}$$

where σ_p and σ_n are the electrical conductivities of the valence (p) and conduction (n) bands (VB and CB, respectively), while S_p and S_n are the Seebeck coefficients for the VB and CB, respectively.

The details of the κ_{bp} calculations are provided with the two-band model analysis in the Supplementary Materials, while the results of the calculations are shown in Figure 4c. The κ_{bp} value was gradually reduced from 0.36 to 0.23 W/m·K at 480 K, which represents a 36% decrease. The decrease in κ_{bp} is also mostly related to the increased concentration of electron carriers, which are the majority carriers. Therefore, the influence of the minority carriers is reduced. The inset of Figure 4c highlights a linear relationship between the κ_{bp} and σ_p values at 480 K [21]. The σ_p values estimated from the two-band model are provided in the Supplementary Materials and Table S1.

Then, the κ_{latt} were deduced by subtracting the κ_{elec} and κ_{bp} values from the measured κ_{tot}, and are shown as symbols in Figure 4d. The κ_{latt} (symbols in Figure 4d) was fitted to the theoretical κ_{latt} (lines in Figure 4d) using the Debye-Callaway equation:

$$\kappa_{latt} = \frac{k_B}{2\pi^2 v}\left(\frac{k_B T}{h}\right)^3 \int_0^{\theta_D/T} \tau_{tot}(z)\frac{z^4 e^z}{(e^z-1)^2}dz \tag{5}$$

where τ_{tot}, θ_D, v, and $\hbar$ are the total phonon relaxation time, Debye temperature, phonon group velocity, and Planck constant divided by 2π, respectively, while $z = \hbar\omega/k_BT$ (ω = phonon frequency). Therefore, the determined $\tau_{tot}(z)$ values describe the theoretical κ_{latt}, whereas $\tau_{tot}(z)$ can be estimated from the individual phonon relaxation times (τ_i) for scattering mechanisms, based on Matthiessen's equation (Equation (6)):

$$\tau_{\text{total}}(z)^{-1} = \sum_i \tau_i(z)^{-1} = \tau_U(z)^{-1} + \tau_B(z)^{-1} + \tau_{PD}(z)^{-1}. \quad (6)$$

For scattering by point defects, which is the dominant mechanism in the present Pd doping case, the phonon relaxation time can be described using the scattering parameter (Γ) within τ_{PD}, as shown in Equations (7) and (8):

$$\tau_{PD}{}^{-1} = P\, f(1-f)\, \omega^4 = \frac{V\omega^4}{4\pi v^3}\Gamma \quad (7)$$

$$\Gamma = f(1-f)\left[\left(\frac{\Delta M}{M}\right)^2 + \frac{2}{9}\left\{(G+6.4\gamma)\frac{1+r}{1-r}\right\}^2\left(\frac{\Delta a}{a}\right)^2\right]. \quad (8)$$

In Equation (7), P and f are a fitting parameter and substituting fraction, respectively. In Equation (8), ΔM and Δa are the difference in mass and lattice constant between the two constituents of an alloy. The G and γ represent the ratio of the fractional change in the bulk modulus to the local bond length and the Grüneisen parameter, while r is the Poisson ratio. Further details of the calculation were not included here, because we found no differences in the κ_{latt} values.

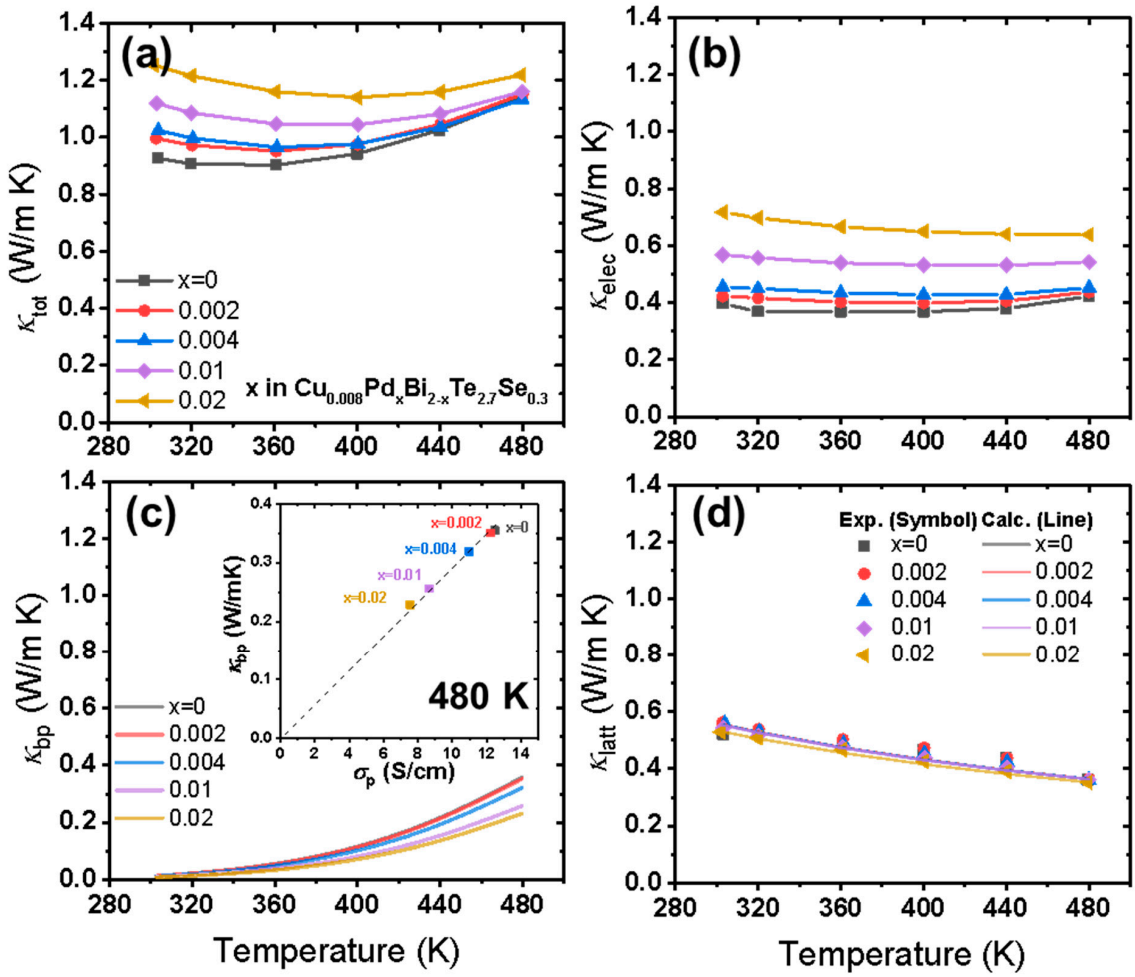

Figure 4. (**a**) κ_{tot} ($\kappa_{tot} = \kappa_{elec} + \kappa_{latt} + \kappa_{bp}$), (**b**) κ_{elec}, (**c**) κ_{bp}, and (**d**) κ_{latt}. The inset of (**c**) shows the linear relationship between κ_{bp} and σ_p.

The theoretical κ_{latt} is shown as solid lines in Figure 4d, along with the experimental κ_{latt} (symbols). The experimental or theoretical κ_{latt} values show rather small changes with the doping level, despite reaching a maximum at $x = 0.02$, implying that only minor additional scattering originated from the doped Pd. This is a peculiar result, as there is much evidence of additional point defect scattering upon substitutional doping. Due to the effect of the mass and lattice constant differences between two constituents of an alloy, described by Equation (8), we would expect a rather large additional contribution from phonon scattering, due to the large mass and ionic radius differences between Pd and Bi (M_{Pd} = 106.42 u, M_{Bi} = 208.98 u, r_{Pd} = 90 pm, r_{Bi} =117 pm). Despite the rather large ΔM and Δa values, we did not observe significant additional scattering due to the Pd doping. A possible explanation would be that intercalated Cu and Te/Se disorder already provide enough point defect scattering, so that Pd substitution would not contribute further in reducing κ_{latt}. Scattering from Cu is known to be rather effective [12]. Consequently, the κ_{tot} value at 300 K showed a significant increase due to the increased κ_{elec}, whereas that at 480 K increased only slightly, together with the decrease in κ_{bp}, seen in Figure 4a.

Figure 5 shows the zT values of all samples. At low temperatures, the zT values were reduced, mainly due to the κ_{tot} increase. However, at higher temperatures (over 400 K), enhanced zT values were observed for intermediate Pd doping levels of $x = 0.004$ and 0.01. This is due to the enhanced power factors, along with the fact that κ_{tot} did not increase significantly despite the κ_{elec} increase. For instance, the zT at 480 K increased from 0.70 to 0.79 in the $x = 0.01$ case. However, no clear Pd doping-induced enhancement in zT was observed at doping levels higher than $x = 0.01$, due to the simultaneous increase in κ_{elec} and κ_{tot}, resulting from an excessive increase in electron carrier concentration. We found that moderate doping of Pd with levels of x = 0.004 to 0.01 in *n*-type $Cu_{0.008}Bi_2Te_{2.7}Se_{0.3}$ can be effective in enhancing the power factor. However, the Pd doping in Cu-doped *n*-type $Bi_2(Te,Se)_3$ did not further reduce κ_{latt} despite the rather large ΔM and Δa values.

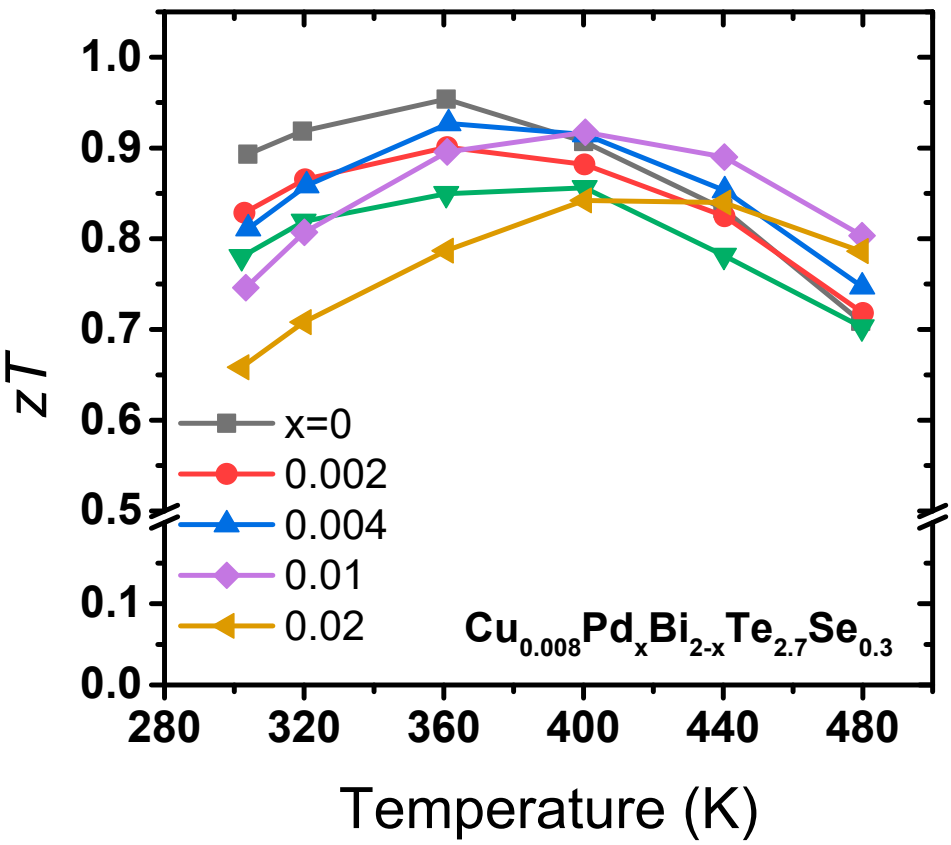

Figure 5. zT values of $Cu_{0.008}Pd_xBi_{2-x}Te_{2.7}Se_{0.3}$ (x = 0, 0.002, 0.004, 0.01, and 0.02).

4. Conclusions

We studied the influence of Pd substitution in *n*-type Cu-doped $Bi_2Te_{2.7}Se_{0.3}$, $Cu_{0.008}Bi_2Te_{2.7}Se_{0.3}$, by analyzing the electrical and thermal properties of a series of *n*-type $Cu_{0.008}Pd_xBi_{2-x}Te_{2.7}Se_{0.3}$ alloys (x = 0, 0.002, 0.004, 0.01, and 0.02) based on a single parabolic band and Debye-Callaway models. As the Pd doping increased, the electron carrier concentration and electrical conductivity increased simultaneously. The power factor was also enhanced, especially at higher temperatures. The bipolar conduction in the Pd-doped $Cu_{0.008}Bi_2Te_{2.7}Se_{0.3}$ samples was reduced; in particular, the bipolar thermal conductivity showed a significant decrease from 0.36 W/m·K in the undoped sample to 0.24 W/m·K in the x = 0.02 doped sample at 480 K. However, the analysis of the lattice thermal conductivity showed that substitutional Pd is not very effective in enhancing phonon scattering when interstitial Cu and Se/Te disorder are already present. Consequently, enhanced zT values at temperatures higher than 400 K were observed for the x = 0.004 and 0.01 doped samples.

Supplementary Materials: The following are available online at http://www.mdpi.com/1996-1944/12/24/4080/s1, Table S1 Band parameters of Pd-doped $Cu_{0.008}Pd_xBi_{2-x}Te_{2.7}Se_{0.3}$ samples (x = 0, 0.002, 0.004, 0.01, and 0.02) calculated using the two-band model.

Author Contributions: Conceptualization, W.H.S.; Formal analysis, Y.O. and Y.Y.; Investigation, H.-j.C., S.-s.C., and S.-w.H.; Methodology, K.L. and J.-H.L., S.-M.C.; Project administration, S.-i.K.; Supervision, W.H.S., K.H.L.; Writing—original draft, S.Y.K., H.-S.K. and S.-i.K.; Writing—review and editing, H.J.P. and K.H.L.

Funding: This research was funded by the 2018 Research Fund of the University of Seoul (20180511069).

Conflicts of Interest: The authors declare no conflict of interest" or declare any conflicts of interest.

References

1. Bell, L.E. Cooling, heating, generating power, and recovering waste heat with thermoelectric systems. *Science* **2008**, *321*, 1457–1461. [CrossRef] [PubMed]
2. Scherrer, H.; Scherrer, S. *Thermoelectrics Handbook: Macro to Nano*, 1st ed.; Rowe, D.M., Ed.; CRC Press: Boca Raton, FL, USA, 2006; pp. 1–27.
3. Cui, J.; Xiu, W.; Xue, H. High thermoelectric properties of p-type pseudobinary $(Cu_4Te_3)_x$–$(Bi_{0.5}Sb_{1.5}Te_3)_{1-x}$ alloys prepared by spark plasma sintering. *J. Appl. Phys.* **2007**, *101*, 123713. [CrossRef]
4. Mun, H.; Lee, K.H.; Kim, S.J.; Kim, J.Y.; Lee, J.H.; Lim, J.H.; Park, H.J.; Roh, J.W.; Kim, S.W. Fe-Doping Effect on Thermoelectric Properties of p-Type $Bi_{0.48}Sb_{1.52}Te_3$. *Materials* **2015**, *8*, 959–965. [CrossRef] [PubMed]
5. Kim, H.S.; Lee, K.H.; Yoo, J.Y.; Shin, W.H.; Roh, J.W.; Hwang, J.Y.; Kim, S.W.; Kim, S.I. Suppression of bipolar conduction via bandgap engineering for enhanced thermoelectric performance of p-type $Bi_{0.4}Sb_{1.6}Te_3$ alloys. *J. Alloy. Compd.* **2018**, *741*, 869–874. [CrossRef]
6. Lee, K.H.; Hwang, S.W.; Ryu, B.K.; Ahn, K.H.; Roh, J.W.; Yang, D.J.; Lee, S.M.; Kim, H.S.; Kim, S.I. Enhancement of the Thermoelectric Performance of $Bi_{0.4}Sb_{1.6}Te_3$ Alloys by In and Ga Doping. *J. Electron. Mater.* **2013**, *42*, 1617–1621. [CrossRef]
7. Lee, K.H.; Choi, S.M.; Roh, J.W.; Hwang, S.W.; Kim, S.I.; Shin, W.H.; Park, H.J.; Lee, J.H.; Kim, S.W.; Yang, D.J. Enhanced Thermoelectric Performance of p-Type Bi-Sb-Te Alloys by Codoping with Ga and Ag. *J. Electron. Mater.* **2015**, *44*, 1531–1535. [CrossRef]
8. Zhai, R.S.; Wu, Y.H.; Zhu, T.J.; Zhao, X.B. Thermoelectric performance of p-type zone-melted Se-doped $Bi_{0.5}Sb_{1.5}Te_3$ alloys. *Rare Met.* **2018**, *37*, 308–315. [CrossRef]
9. Kim, H.; Lee, J.K.; Park, S.D.; Ryu, B.K.; Lee, J.E.; Kim, B.S.; Min, B.K.; Joo, S.J.; Lee, H.W.; Cho, Y.R. Enhanced thermoelectric properties and development of nanotwins in Na-doped Bi0.5Sb1.5Te3 alloy. *Electron. Mater. Lett.* **2016**, *12*, 290–295. [CrossRef]
10. Kim, I.H.; Choi, S.M.; Seo, W.S.; Cheong, D.I. Thermoelectric properties of Cu-dispersed $Bi_{0.5}Sb_{1.5}Te_3$. *Nanoscale Res. Lett.* **2012**, *7*, 2. [CrossRef] [PubMed]
11. Kim, H.S.; Lee, K.H.; Yoo, J.Y.; Youn, J.H.; Roh, J.W.; Kim, S.I.; Kim, S.W. Effect of substitutional Pb doping on bipolar and lattice thermal conductivity in p-type $Bi_{0.48}Sb_{1.52}Te_3$. *Materials* **2017**, *10*, 763. [CrossRef] [PubMed]

12. Cho, H.J.; Shin, W.H.; Choo, S.S.; Kim, J.I.; Yoo, J.Y.; Kim, S.I. Synergistic Influence of Cu Intercalation on Electronic and Thermal Properties of n-Type $Cu_xBi_2Te_{2.7}Se_{0.3}$ Polycrystalline Alloys. *J. Electron. Mater.* **2019**, *48*, 1951–1957. [CrossRef]
13. Tan, X.; Liu, G.; Xu, J.; Tan, X.; Shao, H.; Hu, H.; Jiang, H.; Lu, Y.; Jiang, J. Thermoelectric properties of In-Hg co-doping in SnTe: Energy band engineering. *J. Mater.* **2018**, *4*, 62–67. [CrossRef]
14. Roychowdhury, S.; Biswas, K. Effect of In and Cd co-doping on the thermoelectric properties of Sn1−xPbxTe. *Mater. Res. Express* **2019**, *6*, 104010. [CrossRef]
15. Cohen, I.; Kaller, M.; Komisarchik, G.; Fuks, D.; Gelbstein, Y. Enhancement of the thermoelectric properties of n-type PbTe by Na and Cl co-doping. *J. Mater. Chem. C* **2015**, *3*, 9559–9564. [CrossRef]
16. Kihoi, S.K.; Kim, H.; Jeong, H.; Kim, H.; Ryu, J.; Yi, S.; Lee, H.S. Thermoelectric properties of Mn, Bi, and Sb co-doped SnTe with a low lattice thermal conductivity. *Alloys Compd.* **2019**, *806*, 361–369. [CrossRef]
17. Kim, H.-S.; Choo, S.-S.; Cho, H.-J.; Kim, S.-I. Beneficial Influence of Co-Doping on Thermoelectric Efficiency with Respect to Electronic and Thermal Transport Properties. *Phys. Status Sol. A* **2019**, *216*, 1900039. [CrossRef]
18. May, A.F.; Snyder, G.J. *Materials, Preparation, and Characterization in Thermoelectric*; Rowe, D.M., Ed.; CRC Press: Boca Raton, FL, USA, 2012; pp. 1–11.
19. Callaway, J. Model for Lattice Thermal Conductivity at Low Temperatures. *Phys. Rev.* **1959**, *113*, 1046. [CrossRef]
20. Kim, H.S.; Gibbs, Z.M.; Tang, Y.; Wang, H.; Snyder, G.J. Characterization of Lorenz number with Seebeck coefficient measurement. *APL Mater.* **2015**, *3*, 041406. [CrossRef]
21. Wang, S.; Yang, J.; Toll, T.; Yang, J.; Zhang, W.; Tang, X. Conductivity-limiting bipolar thermal conductivity in semiconductors. *Sci. Rep.* **2015**, *5*, 10136. [CrossRef] [PubMed]